Supporting Information for

Fluorescent Drug-Loaded Polymeric-Based Branched Gold Nanoshells for Localised Multimodal Therapy and Imaging of Tumoral Cells

Antonio Topete[1], Manuel Alatorre-Meda[1, †,#], Pablo Iglesias[2], Eva M. Villar-Alvarez[1], Silvia Barbosa[1,], José A. Costoya[2], Pablo Taboada[1,*], Víctor Mosquera[1]*

[1] Grupo de Física de Coloides y Polímeros, Departamento de Física de la Materia Condensada, Universidad de Santiago de Compostela, Santiago de Compostela, 15782, Spain.

[2] Grupo de Oncología Molecular, Centro de Investigación en Medicina Molecular y Enfermedades Crónicas (CIMUS), Universidad de Santiago de Compostela, Santiago de Compostela, 15782, Spain.

[#]Present address: 3B's Research Group-Biomaterials, Biodegradables and Biomimetics, University of Minho, Headquarters of the European Institute of Excellence on Tissue Engineering and Regenerative Medicine, AvePark, Zona Idustrial da Gandra, S. Claudio do Barco, Caldas das Taipas, Guimarães, 48-909, Portugal.

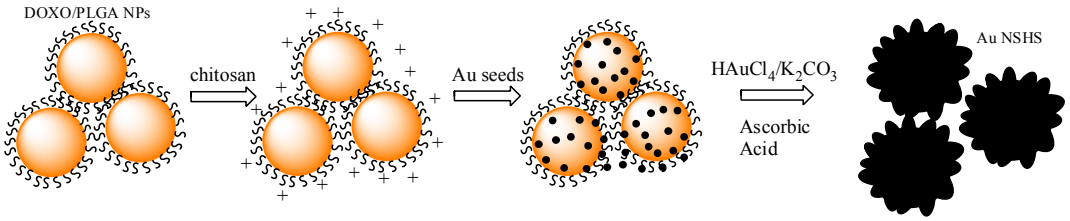

Figure S1: Scheme of the production of BGNSHs. First DOXO-loaded PLGA NPs (~80 nm) were prepared by a nanoprecipitation method. These solid spheres were functionalized with chitosan chains to bind negatively charged citrated-Au seeds. Finally, the PLGA NP-seed precursor was used as substrate to grow branched Au nanoshells, which resemble virus structures.

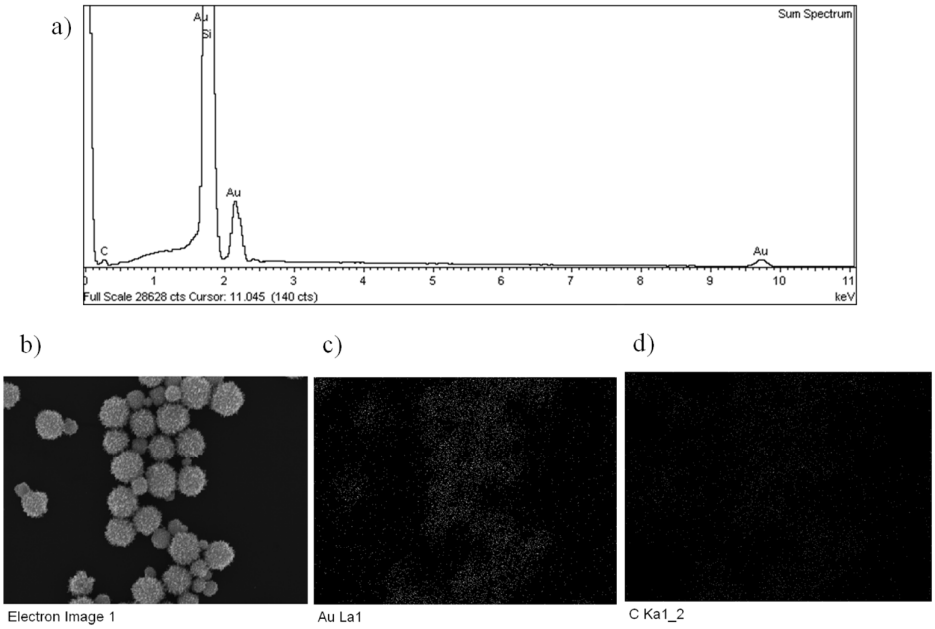

Figure S2: a) EDX spectrum of BGNSHs with an Au peak from the shell and a small C peak form the PLGA core. A shoulder corresponding to O might be also present. b) SEM image and bit maps of c) Au and d) C atoms. This maps show that both elements coincide at the same regions, which can be interpreted as the Au shell is porous.

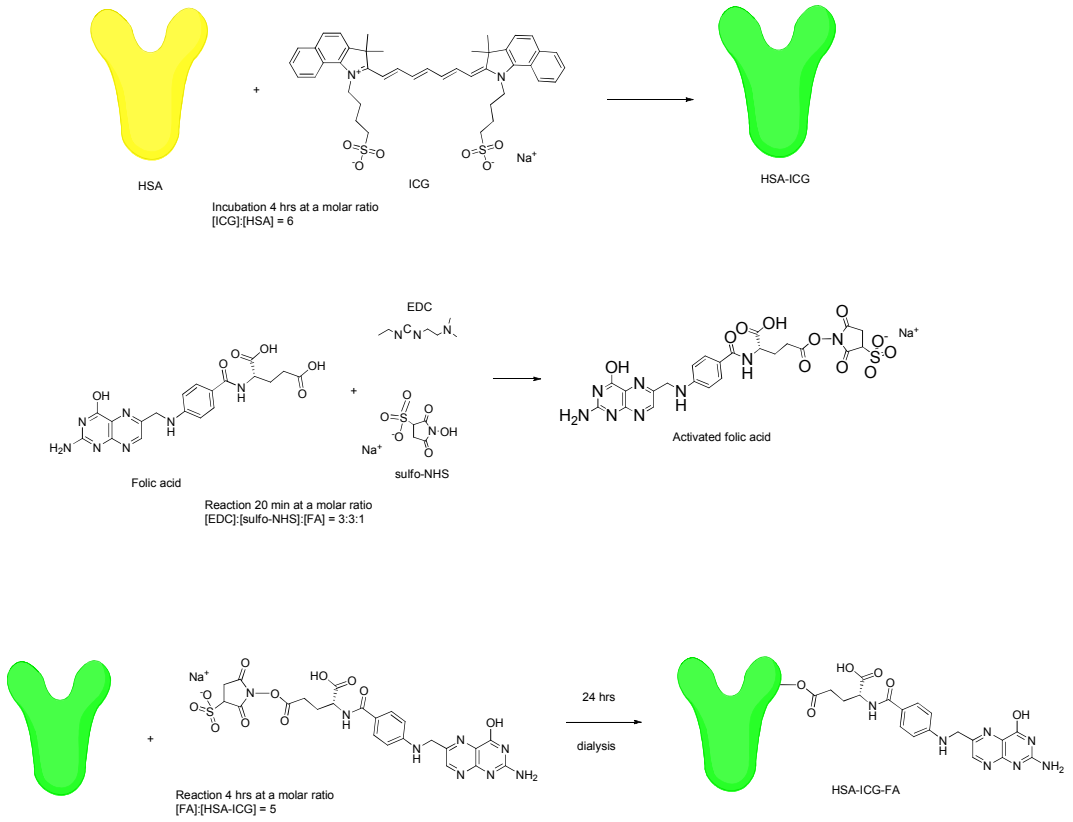

Figure S3: Scheme of the conjugation of ICG and folic acid to HSA.

Table S1: Zeta potential of HSA complexes in MES 50 μM (pH 6)

Sample	Zeta Potential (mV)
HSA	-5.6 ± 0.4
HSA-ICG	-1.0± 0.9
HSA-ICG-FA	-27.6 ± 1.7

Table S2: Hydrodynamic radius and zeta potential of BGNSHs in PBS 10 mM (pH 7.4)

Sample	r_h (nm)	Zeta Potential (mV)
Bare BGNSHs	55.2 ± 4.9	-24.6 ± 1.8
BGNSH-HSA	67.1 ± 8.9	-20.9 ± 2.4
BGNSH-HSA-ICG	68.1 ± 14.6	-16.6 ± 1.2
BGNSH-HSA-ICG-FA	68.3 ± 12.3	-16.3 ± 1.7

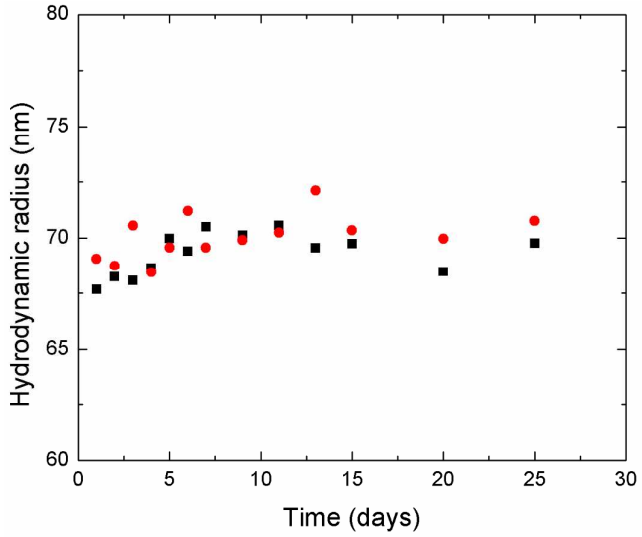

Figure S4: Size stability of BGNSH-HSA-ICG-FA nanoplatforms with time at (■) PBS buffer of PH 7.4 supplemented with 10% (v/v) FBS, and (●) in pure FBS, respectively.

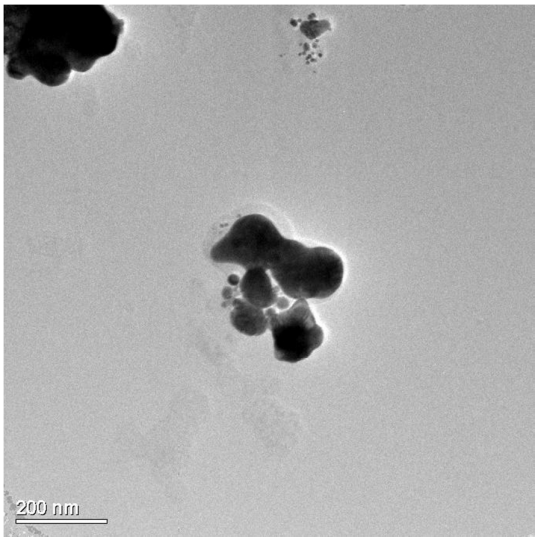

Figure S5: TEM image of a BGNSH-HSA-ICG-FA nanoplatform after 30 min of irradiation at 10 W cm^{-2}.

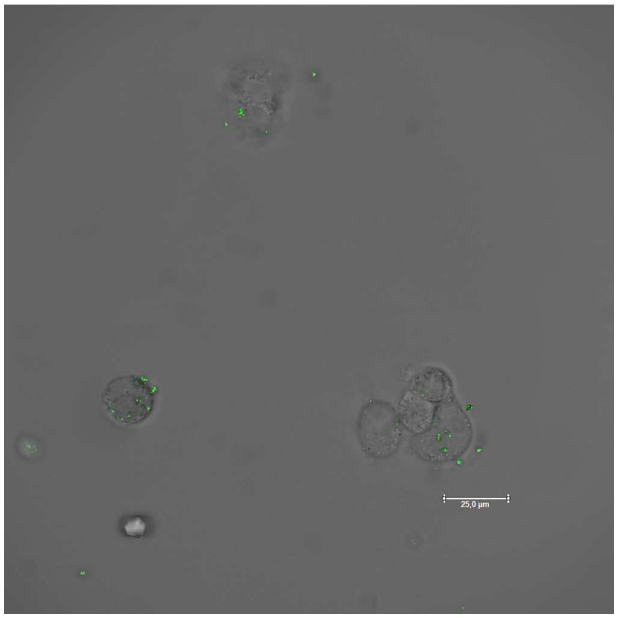

Figure S6: Merged confocal NIR images of BGNSH-HSA-ICG-FA nanoplatform internalization inside MDA-MB-231 breast cancer cells.

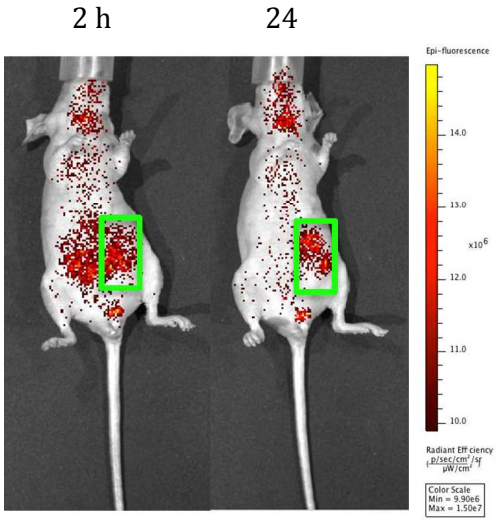

Figure S7: Biodistribution and localization of BGNSH-HSA-ICG nanoplatforms at the tumor site (denoted by the green-squeared region in the images) after 2 and 24 h after injection.

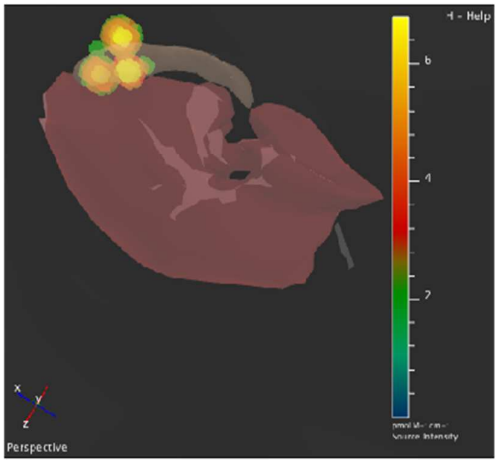

Figure S8: 3D-reconstructed fluorescence images of accumulation in the RES system after 12 h of incubation in a MDA-MB-231 tumor-bearing mouse after intravenous tail injection of BGNSH-HSA-ICG-FA nanoplatforms.

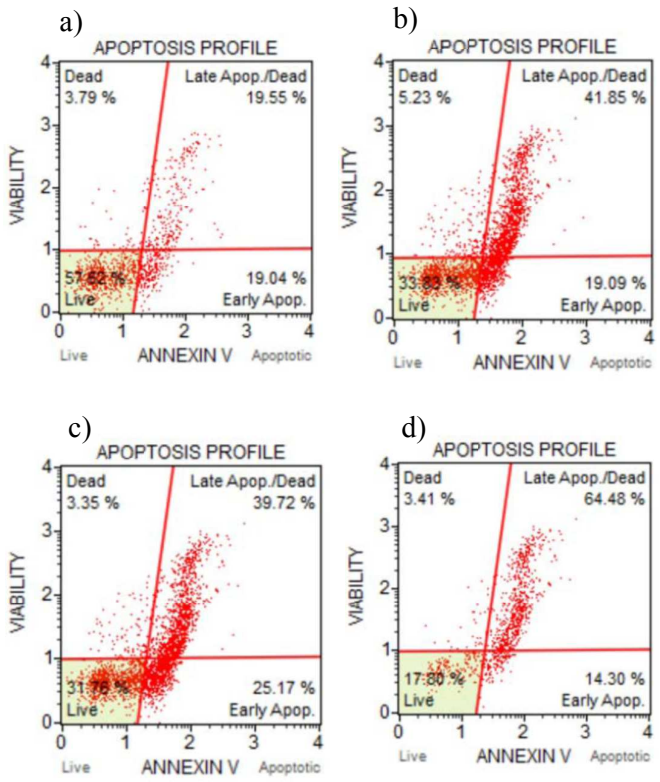

Figure S9: Annexin V/Dead Cell flow cytometry profiles of a) BGNSH-HSA, b) BGNSH-HSA-ICG, c) BGNSH-HSA-ICG-FA and d) DOXO-BGNSH-HSA-ICG-FA.

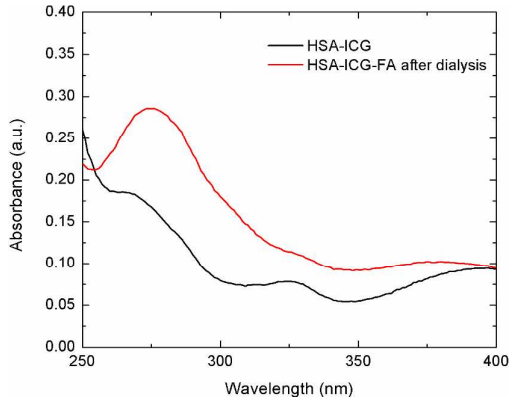

Figure S10: UV-vis spectra of HSA-ICG complexes before and after reaction/dyalisis with FA*.

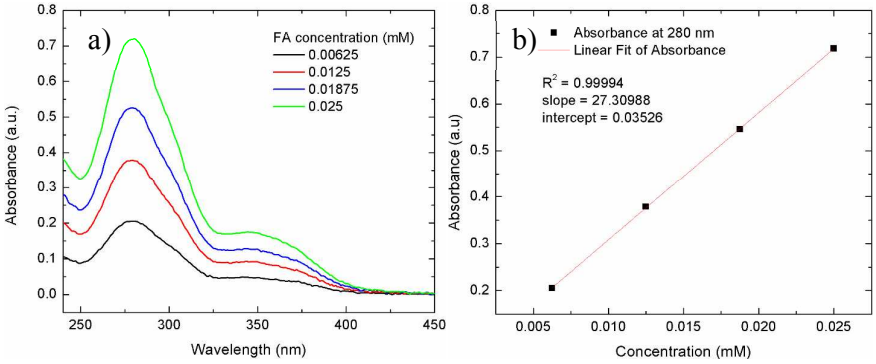

Figure S11: a) UV-vis spectra and calibration curve of FA, and b) linear fit of absorbance at 280 *vs.* FA concentration.